Alary muscles and thoracic alary-related muscles are atypical striated muscles involved in maintaining the position of internal organs

Laetitia Bataillé, Nathalie Colombié, Aurore Pelletier, Achim Paululat, Gaëlle Lebreton, Yannick Carrier, Jean-Louis Frendo, Alain Vincent

© 2020. Published by The Company of Biologists Ltd | Development (2020) 147, dev185645. doi:10.1242/dev.185645

RESEARCH ARTICLE

Alary muscles and thoracic alary-related muscles are atypical striated muscles involved in maintaining the position of internal organs

Laetitia Bataillé[1,*], Nathalie Colombié[1], Aurore Pelletier[1], Achim Paululat[2], Gaëlle Lebreton[1], Yannick Carrier[1], Jean-Louis Frendo[1] and Alain Vincent[1]

ABSTRACT

Alary muscles (AMs) have been described as a component of the cardiac system in various arthropods. Lineage-related thoracic muscles (TARMs), linking the exoskeleton to specific gut regions, have recently been discovered in *Drosophila*. Asymmetrical attachments of AMs and TARMs, to the exoskeleton on one side and internal organs on the other, suggested an architectural function in moving larvae. Here, we analysed the shape and sarcomeric organisation of AMs and TARMs, and imaged their atypical deformability in crawling larvae. We then selectively eliminated AMs and TARMs by targeted apoptosis. Elimination of AMs revealed that AMs are required for suspending the heart in proper intra-haemocelic position and for opening of the heart lumen, and that AMs constrain the curvature of the respiratory tracheal system during crawling; TARMs are required for proper positioning of visceral organs and efficient food transit. AM/TARM cardiac versus visceral attachment depends on Hox control, with visceral attachment being the ground state. TARMs and AMs are the first example of multinucleate striated muscles connecting the skeleton to the cardiac and visceral systems in bilaterians, with multiple physiological functions.

KEY WORDS: Alary muscles, Striated muscles, Cardiac system, Respiratory system, Visceral system, *Drosophila*

INTRODUCTION

Three types of muscles are classically distinguished in mammals: skeletal, cardiac and smooth muscle. The cardiac and skeletal muscles are striated, with striation reflecting the reiteration of sarcomeres, which are the basic contractile units assembled from alternating antiparallel rows of myosin-based thick and actin-based thin filaments. Skeletal muscle fibres, which underlie body movements, are multinucleated syncytia formed by fusion of myocytes. They attach to the skeleton via tendons at both ends, except for some facial muscles and extra-ocular muscles, which either attach to the epidermis or to other muscles (Pélissier et al., 2000; Noden and Francis-West, 2006; Ziermann et al., 2018). Holometabolous insects display two successive muscle patterns, which underlie larval and adult locomotion. Locomotion of the soft-bodied *Drosophila* larva includes linear crawling, head turns and rolling movements (Hwang et al., 2007; Heckscher et al., 2012). About 30 distinct body wall muscles per hemi-segment are attached at both ends to the larval exoskeleton via tendon cells (Bate and Rushton, 1993; Armand et al., 1994). Each muscle displays a specific morphology, which is linked to the expression of muscle identity transcription factors (iTFs), including many orthologues of mammalian myogenic TFs, such as MyoD/MRF, Islet1, Six and Tbx1 (de Joussineau et al., 2012; Dubois et al., 2016; Buckingham, 2017). Beside the muscles required for locomotion, one alary muscle (AM) in each abdominal hemi-segment connects the lateral exoskeleton to the dorsal vessel, the *Drosophila* cardiac system which comprises the aorta and the heart. At larval hatching, seven pairs of AMs adhere to the extracellular matrix (ECM) surrounding the pericardial cells (PCs) located along the aorta and heart proper (Rizki, 1978; LaBeau et al., 2009; Lehmacher et al., 2012). Org-1 (Optomotor-blind-related-gene-1), the *Drosophila* Tbx1 orthologue, and Tailup (Tup)/Islet1 are iTFs expressed in AMs (Tao et al., 2007; Schaub et al., 2012; Boukhatmi et al., 2012). Characterisation of *Org-1* and *tup* mesodermal enhancers led us to discover the existence of three pairs of thoracic alary-related muscles (TARMs), each attaching to a specific midgut region (Fig. 1A,B and Boukhatmi et al., 2014).

AMs have been described in many arthropods and proposed to connect epi/pericardial cells around the adult heart and to control ostia opening and heart beating (Jones, 1954; Curtis et al., 1999; Ejaz and Lange, 2008; Buechling et al., 2009; Glenn et al., 2010; League et al., 2015), although neither role has been formally established. Moreover, the finding that adhesion of one AM to the distal tip cell of Malpighian tubules (MTs) is required for proper MT bending during embryogenesis (Weavers and Skaer, 2013) and that AMs and TARMs loop around main branches of the respiratory tracheal system (Boukhatmi et al., 2014) led us to postulate a function of AMs and TARMs in internal organ positioning in crawling larvae (Bataillé et al., 2015).

Here, we analysed in detail the striated organisation of AMs/TARMs and their attachments to multiple internal organs, and imaged their deformability in crawling larvae. We then ablated AMs and TARMs by transcription enhancer-targeted apoptosis. Loss of AMs induces a collapse of the cardiac system and relieves topological constraints on the curvature of the respiratory system. Loss of TARMs interferes with positioning of the gastric caeca and visceral mass and affects food transit. Our characterisation of TARMs/AMs, a new type of muscle connecting the skeleton to internal organs with multiple physiological functions, brings a new viewpoint on animal anatomy.

RESULTS

Morphological diversification of AMs and TARMs: Hox control

Pan-mesodermic expression of the homeotic protein Ubx induces transformation of TARMs into AM-like muscles connecting to

[1]Centre de Biologie du Développement (CBD), Centre de Biologie Intégrative (CBI), Université de Toulouse 3, CNRS, UPS, 118 route de Narbonne, 31062 Toulouse, France. [2]University of Osnabrück, Department of Biology/Chemistry, Zoology and Developmental Biology, Barbarastraße 11, 49076 Osnabrück, Germany.

*Author for correspondence (laetitia.bataille@univ-tlse3.fr; laetitia.bataille@inserm.fr)

L.B., 0000-0002-3897-9520; N.C., 0000-0002-6239-7109; J.-L.F., 0000-0003-0118-5556; A.V., 0000-0002-2769-7501

Received 15 October 2019; Accepted 4 March 2020

Development (2020) 147, dev185645. doi:10.1242/dev.185645

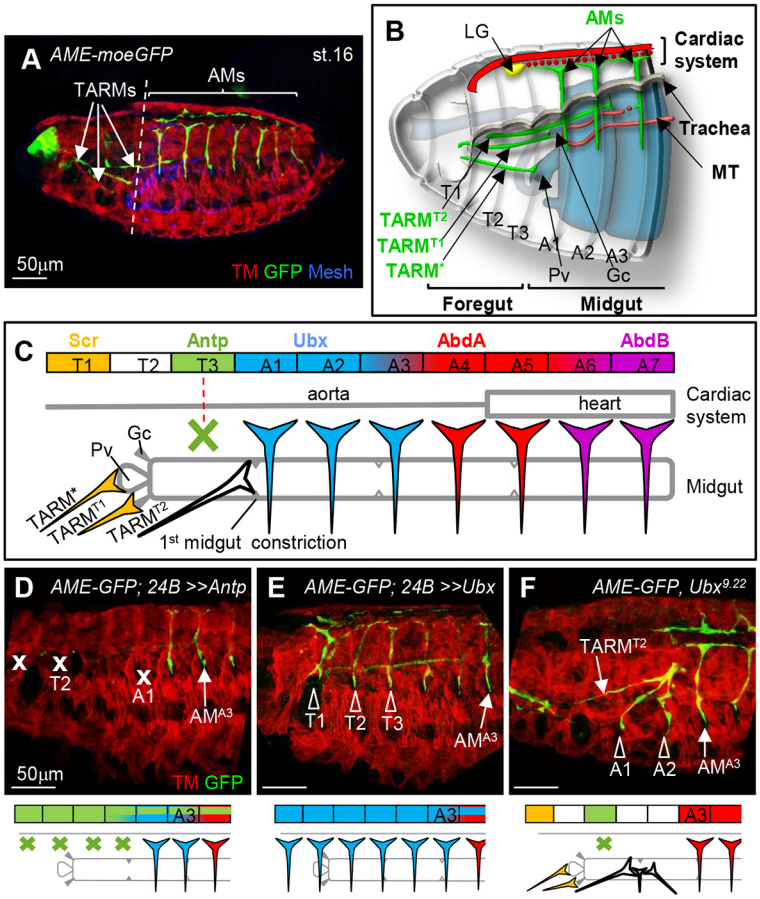

Fig. 1. Hox control of TARM and AM internal organ connections. (A) Stage 16 *AME-moeGFP* embryo stained for GFP (green), Tropomyosin (TM, red) and Mesh (blue) to visualise the AMs and TARMs, somatic muscles, and gut, respectively. (B) Schematic of the anterior region of a stage 16 embryo, showing AMs (green) connections to the cardiac system (red), lymph gland (LG, yellow) and tip cell of the Malpighian tubule (MT, orange). AMs run internal to the dorsal tracheal trunk (grey). TARM*, TARM^{T1} and TARM^{T2} span several segments and connect to the proventriculus (Pv), dorsal gastric caeca (Gc) and first midgut constriction, respectively. Scheme modified from Boukhatmi et al. (2014). (C) Colour-coded representation of Scr, Antp, Ubx, AbdA and AbdB expression in TARMs/AMs and of TARM and AM connections to specific midgut regions and the cardiac system in wild-type embryos. The green cross indicates muscle death induced by Antp expression. (D-F) Anterior region of *AME-moeGFP; 24B-Gal4/UAS-Antp* (D), *AME-moeGFP; 24B-Gal4/UAS-Ubx* (E) and *AME-moeGFP, Ubx$^{9.22}$* (F) embryos stained for GFP and TM (see A). AM^{A3} position, and ablated (x) or transformed (arrowhead) muscles are indicated. Below are schematic representations of the observed AM/TARM transformations (n>30). Scale bars: 50 µm.

the aorta (LaBeau et al., 2009; Weavers and Skaer, 2013; Bataillé et al., 2015), the first indication that Hox activity distinguishes between AM and TARM morphology and their attachment to either the circulatory or the visceral system. To investigate this in depth, we surveyed Hox expression in TARMs and AMs (Fig. 1C; Fig. S1). TARM* and TARM^{T1}, which connect the proventriculus (Pv) and dorsal gastric caeca (Gc), respectively, originate from progenitor cells specified in T1 and express Scr. No Hox expression could be detected in TARM^{T2}, which connects to the first midgut constriction, and Antp is expressed in the abortive TARM^{T3}, which undergoes apoptosis during embryogenesis (Fig. S1). Abdominal AMs express the Bithorax complex proteins Ubx in A1-A3, AbdA in A3-A7 (LaBeau et al., 2009) and AbdB in A5-A7 segments.

The TARM/AM Hox code raised the question of whether Antp expression induces TARM apoptosis. Ectopic Antp expression in the entire mesoderm results in loss of all TARMs plus, in most embryos, AM^{A1} (Fig. 1D). Conversely, as previously reported (Bataillé et al., 2015), Ubx pan-mesodermal expression induces formation of an AM-like muscle in T3 (Fig. 1E). Thus, Antp promotes TARM^{T3} apoptosis in the absence of posterior Hox function. The absence of Hox expression in TARM^{T2} is reminiscent of the situation reported for somatic muscles by Roy et al. (1997), who proposed that the T2 muscle pattern was a 'ground state'. To analyse this further, we examined *Ubx* loss-of function embryos. Absence of Hox information leads to AM^{A1} and AM^{A2} transformation into TARM-like muscles connecting to the gut (21/34 hemi-embryos, 62%) at the same position as TARM^{T2} (Fig. 1F). Together, Hox expression, loss-of-function and gain-of-function phenotypes show both that the number of TARMs and attachment of TARMs and AMs to either the visceral or circulatory systems are under Hox control, and that the background state is visceral attachment.

AMs and TARMs connect to multiple internal organs in larvae

AMs have been described as a structural component of the adult insect heart, but their physiological role has never been analysed. One essential step towards addressing TARM/AM functions in larvae is examining their morphology. One plausible reason why TARMs were only recently discovered is their unusual thinness and internal position (Boukhatmi et al., 2014). To circumvent any possible damage to TARMs/AMs during dissections, we engineered fluorescent transgenes *AME$_R$-cd4-tandem(td)Tomato* or *-cd4-tdGFP* in order to visualise AMs and TARMs in intact larvae (Fig. 2; Fig. S2). These tags revealed that TARMs and AMs maintain their connections to specific internal organs throughout larval development. However, although all AMs display a similar morphology in embryos (Fig. 1A), the anterior AMs connecting to the aorta (A1-A4 segments) adopt a conspicuous 'T' shape in larvae (Fig. 2A); the shaft runs from lateral tendon cells to the aorta, whereas lateral branches run orthogonally along the aorta. Each A1-A4 AM thus connects to a specific number of PCs [AM^{A1}: 1 PC; AM^{A2}: 1.7±0.7; AM^{A3}: 3.3±0.8; AM^{A4}: 4.4±0.5 (n=24)]. AM^{A1} also connects to the primary lobe of the lymph gland (LG), the larval haematopoietic organ, and vesicles originating from AMs are observed in the aorta in this region (Fig. S3). AM^{A2} and AM^{A3} connect to secondary, posterior LG lobes (Fig. S3). Posterior AMs (A5-A7 segments) maintain delta-shaped connections to PCs distributed along the heart, with AM^{A5} connecting to three PCs (3.2±0.5), AM^{A6} to four (4.1±0.5) and AM^{A7} to one PC (1.1±0.3) (n=24). Quadruple labelling of semi-intact larvae, including Pericardin (Prc), a cardiac ECM component

Development (2020) 147, dev185645. doi:10.1242/dev.185645

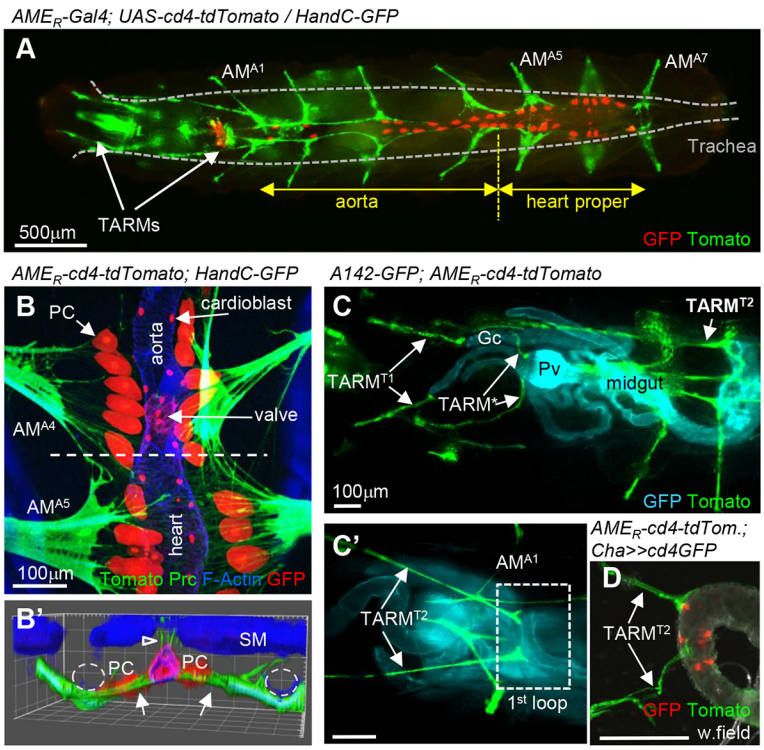

Fig. 2. AMs and TARMs connect to multiple larval internal organs. (A) Dorsal view of an intact *AME$_R$-Gal4; UAS-cd4-tdTomato, HandC-GFP* L3 larva, showing AMs and TARMs in green and PCs, cardioblasts and valve cells in red. Grey dashed lines indicate the position of the dorsal tracheal trunks. (B) AM$^{A4\text{-}A5}$ region of an *AME$_R$-cd4-tdTomato; HandC-GFP* L3 larva stained for Prc and F-Actin, showing PCs and cardioblasts (red), cardiac ECM and AMs (green) and sarcomeres of AMs, somatic muscles and the heart (blue). (B′) 3D reconstructed transversal view of the heart at the position of the dashed line in B, showing the positions of AMs, ECM (green), heart (purple/blue), PCs (red) and dorsal somatic muscles (SM, blue). Dashed circles delineate the tracheal dorsal trunks. ECM connects the heart to AMs (arrow) and to the dorsal epidermis (arrowhead). (C,C′) Dorsal view of the anterior region of an intact *AME$_R$-cd4-tdTomato; A142-GFP* L3 larva showing the gut (cyan) and TARM*, TARM^{T1} and TARM^{T2} (green). TARM* and TARM^{T1} are connected to the Pv and the Gc, respectively (C); TARM^{T2} are connected to the first loop of the midgut (C′). D shows magnification of boxed area in C′. (D) *AME$_R$-cd4-tdTomato; Cha-Gal4, UAS-cd4-tdGFP* larva showing TARM^{T2} connection to DH31-expressing enteroendocrine cells. Scale bars: 500 µm in A; 100 µm in B-D.

(Lehmacher et al., 2012), shows that AM attachment is mediated by cardiac ECM that surrounds PCs (Fig. 2B). 3D reconstructions reveal that, in addition to attaching AMs to the heart, ECM also ties the heart to the dorsal wall (Fig. 2B′). Along their path from the exoskeleton to the heart, AMs loop around the dorsal tracheal branch (Fig. 2B′). Moreover, cytoplasmic protrusions at intermediate positions show that AMs adhere to other internal organs: AM^{A3} to the anterior MT (Weavers and Skaer, 2013), AM^{A1} to the anterior fat body, and AM^{A4} and AM^{A5} to the fat body surrounding the male gonad (Fig. S3).

TARM connections to internal organs were originally mapped in the embryo by immunostainings (Boukhatmi et al., 2014). Here, we visualised these connections in larvae by using *AME$_R$-cd4-tdTomato* labelling of AMs/TARMs and *A142-GFP* expression in visceral organs (Buchon et al., 2013). It shows that TARM* remains connected to the Pv, TARM^{T1} to the tip of dorsal Gcs (Fig. 2C) and TARM^{T2} to the first midgut loop, which shows a characteristic U-shaped bending in larvae (Fig. 2C′,D). This bending occurs where enteroendocrine cells, which express the diuretic hormone DH31, marked by ChAT-Gal4 expression, are located, which is at the junction between the anterior and acidic portions of the midgut (LaJeunesse et al., 2010).

Close examination of AM/TARM connections to the lateral epidermis revealed an unexpected morphological diversity of these attachment sites (Fig. S4). Triple staining for AMs/TARMs, tendon cells and the integrin adhesion complex (Ilk-GFP fusion protein), shows that the discrete adhesion zone of AM/TARMs to one tendon cell is extended by a web of ‘filopodia’ reaching beyond the contacted tendon cell. The role of these projections remains to be explored. Moreover, whereas AM^{A1}-AM^{A5} attach to dorsal tendon cells, AM^{A6} and AM^{A7} attach to lateral tendon cells, i.e. at a more ventral position than AM^{A1}-AM^{A5}, possibly relating to different functions of anterior and posterior AMs.

In summary, AMs and TARMs connect the larval epidermis to many multiple internal organs, reinforcing the hypothesis that AMs and TARMs could contribute to maintenance of the internal anatomy of moving larvae.

AMs and TARMs are multinucleated, sarcomeric muscles displaying unique deformability

In somatic muscle fibres, nuclei are uniformly spaced within the fibre (Volk, 2013). To examine myonuclei number and repartition in AMs and TARMs, we expressed simultaneously nuclear RFP-labelled and membrane-associated GFP proteins (Fig. 3A). TARMs contain between three and four nuclei (TARM*: 2.9±0.3; TARM^{T1}: 4.1±0.9; TARM^{T2}: 4.4±0.5; n=10 larvae), evenly distributed along the fibre length. AM^{A1} to AM^{A7} contain five or six nuclei (5.5±1.1; n=20). In anterior AMs with a ‘T’ shape, nuclei are distributed between the shaft and lateral branches. In posterior AMs, nuclei are distributed in a single row, up to the position where the muscle widens to adopt a delta-like morphology. At this point, nuclei are laterally scattered among the myofibrils (Fig. 3A). Thus, repartition of nuclei in TARMs and AMs adapts to their peculiar asymmetric geometry.

The atypical shapes of TARMs and AMs raised the question of how myofibrils are organised in these muscles. We used cd4-Tomato decoration of AM/TARM contours together with *MHC-GFP* (Sarov et al., 2016) and Phalloidin staining of thick and thin filaments, respectively, to visualise the sarcomeric myofibrils. In the anterior AMs (Fig. 3B,B′), myofibrils align with the shaft, before bending 90° to form lateral branches aligning with the aorta. This bending occurs without rupture in the sarcomeric organisation, such that anterior AMs display two perpendicular sarcomeric contraction lines. In posterior AMs (Fig. 3C,C′), myofibrils scatter in a pattern similar to a fan frame to connect the ECM surrounding the heart (see also Fig. 2B and Lehmacher et al., 2012). The sarcomeric region is extended dorsally by thin cellular extensions reaching cardiomyocytes and, sometimes, the opposite AM proteins (Fig. 3C′). The AM sarcomeres were also visualised by the expression of a titin-like

Development (2020) 147, dev185645. doi:10.1242/dev.185645

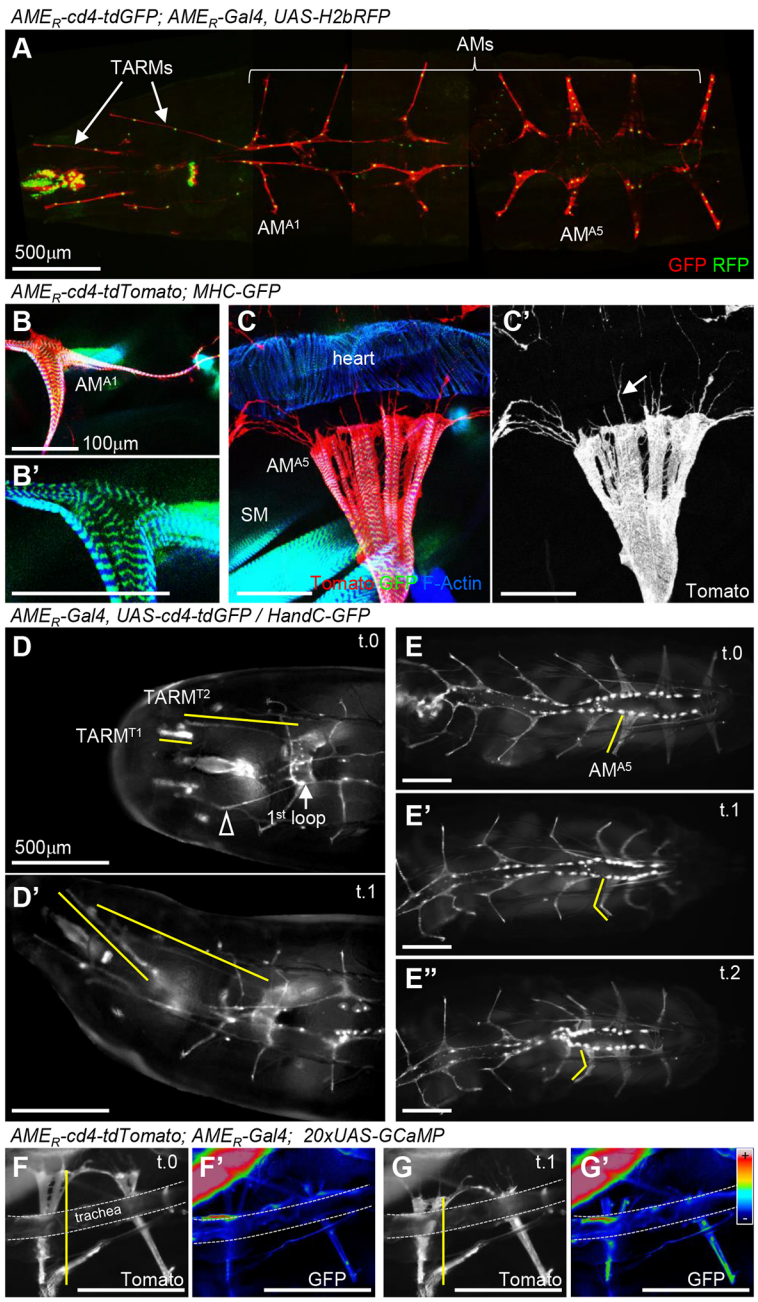

Fig. 3. AMs and TARMs: multinucleated, sarcomeric, deformable muscles. (A) Dorsal view of an *AME$_R$-cd4-tdGFP; AME$_R$-Gal4, UAS-H2bRFP* L3 larva showing the nuclei distribution (green) in AMs and TARMs (red). The image corresponds to a mosaic reconstruction of confocal acquisitions of an entire larva. (B,C) Dissected *AME$_R$-cd4-tdTomato; MHC-GFP* L3 larva, showing the striated structure (MHC-GFP, green; F-Actin, blue) of AM^{A1} (B) and AM^{A5} (C). The heart and somatic muscles (SM) are visible in C. (B′) Magnification of the image shown in B, showing green and blue channels only. (C′) The same image as shown in C but with the red channel only, showing AM^{A5} cytoplasmic protrusions. (D-E″) Snapshots of *AME$_R$-Gal4, UAS-cd4-tdGFP/HandC-GFP* L3 crawling larva, illustrating the deformability of TARMs (D,D′) and AMs (E-E″). Yellow lines indicate TARM^{T1} and TARM^{T2} sizes in contracted (D) and elongated (D′) phases, at two different time points (t0 and t1). The arrowhead in D indicates TARM^{T2} deformation. In E-E″, yellow lines underline AM^{A5} deformations at three successive phases of larval crawling (three time points, t0-t2). (F-G′) Snapshots at two different time points (t0 and t1) of *AME$_R$-cd4-tdTomato; AME$_R$-Gal4; 20xUAS-GCaMP3* larva showing intracellular calcium rise in shortening posterior AMs (n=12). F and G show Tomato staining of AM shape; F′ and G′ show GCaMP fluorescence level in rainbow false colours. Yellow lines indicate AM^{A6} size in its elongated (F) and contracted (G) forms. Scale bars: 500 µm in A, D-G′; 100 µm in B-C′.

protein, the M-line Unc-89-GFP protein; Kettin/Sallimus (Kettin-GFP), a short form of titin linking the Z-disc to myosin filaments (Sarov et al., 2016); and *Zasp66-GFP*, a Z band protein (Hudson et al., 2008). *Zasp66-GFP* expression also indicates the striated structure of TARMs (Fig. S5).

We then imaged TARMs and AMs deformations in living larvae (Fig. 3D-E″; Movies 1 and 2). This revealed the extensibility of TARMs, which are >3-fold longer when extended than when contracted, and are often curved (Fig. 3D,D′), indicating elastic properties. Deformability of AMs is even more peculiar, with three successive shapes along each crawling stride cycle, which comprises a visceral piston phase during which internal organs move asynchronously with surrounding abdominal body wall (Heckscher et al., 2012) (Fig. 3E-E″; Movie 2). AMs (1) are roughly straight, oriented ventral to dorsal in fully elongated larvae, at the start and end of each cycle (Fig. 3E); (2) form an anterior vertex angle during the visceral piston phase, when the gut and tail move forward together (Fig. 3E′); and (3) adopt a reverse, posterior vertex angle, as the peristaltic wave travels from posterior to anterior, during which the abdominal body wall advances (Fig. 3E″). Along this sequence, AMs length varies by about 1.5 times. Detection of a fluorescent calcium indicator, GCaMP3 (Tian et al., 2009), when AMs shorten (Fig. 3F-G′; Movie 3) suggests that they contract upon intracellular calcium release. Whether calcium release drives AM contraction or is a response to mechanical stretching of AMs remains, however, to be deciphered.

Taken together, our data show that TARMs and AMs are both contractile and highly deformable. These unique deformation properties could be linked to their dual attachment to the exoskeleton and internal organs during larval movements. It was thus very important to understand the specific functions of AMs and TARMs.

Development (2020) 147, dev185645. doi:10.1242/dev.185645

AM ablation induces a collapse of the dorsal vessel

To address TARMs and AMs functions in larvae, we devised strategies to eliminate these muscles specifically. Expression of the pro-apoptotic gene *rpr* under control of the AM/TARM *AME$_R$-Gal4* driver (Figs S2 and S6) generates larvae lacking both AMs and TARMs, whereas Antp expression ablates TARMs only (Fig. S6). Either ablation condition led to strong lethality, with only 7.5% *AME$_R$>>rpr* and 14.6% *AME$_R$>>Antp* embryos reaching the end of L3 (Fig. S6; Table S1). Because AMs and TARMs are connected to several internal organs, lethality following their elimination could reflect cumulative defects of larval physiology.

HandC-GFP expression in PCs and cardiomyocytes showed that the number and repartition of PCs is not significantly modified upon *rpr*-induced AM ablation (Fig. 4A-C). However, the left and right PCs rows become juxtaposed along the midline (Fig. 4A-D). We analysed the relative topology of the PCs and heart in semi-intact quadruple-labelled larvae (Fig. 4E-F″). In control larvae, AMs adhere to the ECM surrounding PCs lateral to the heart, and loop around the ventral aspect of the tracheal trunk (Fig. 4E-E″). Upon AM ablation, PCs become pressed against the heart, which itself shifts dorsally. In addition, the heart lumen collapses (Fig. 4F-F″). Prc accumulation in wild-type larvae (Figs 4E′,E″ and 2B′) suggested anchoring of the heart to the dorsal epidermis. Upon Prc depletion, AMs and PCs are no longer tied and come apart from the heart and, at the same time, the heart lumen collapses (Fig. 4G-G″) (Drechsler et al., 2013), as we observed upon AM elimination. However, rather than being shifted dorsally, the heart adopts a more ventral position. Together, the loss-of-AMs and loss-of-ECM phenotypes indicate that forces exerted by AMs and dorsal anchoring ‘suspend’ the heart within the body.

We analysed the heart beating in *HandC-GFP* white pupae (Fig. S7; Movies 4 and 5), a pre-metamorphosis stage when skeletal muscles contractions do not interfere with recording. Upon AM elimination, the heart systolic and diastolic phases strongly decrease. Yet the heart beating rhythm is not affected, indicating that cardiomyocytes retain their full contractility in the absence of AMs, similar to other conditions that prevent haemolymph flux (Choma et al., 2011; Drechsler et al., 2013). We conclude that AMs are not required for larval heart beating per se, but are essential for maintaining proper heart anatomy and, thereby, physiological functions necessitating haemolymph circulation.

AM ablation affects the position of the tracheal trunk

AMs loop around the ventral aspect of the dorsal tracheal trunk (Fig. 4E-E″). When AMs are either eliminated or detached from PCs (Fig. 4F,G), the position of the dorsal tracheal trunk fluctuates in the body cavity. This suggests that AMs sterically constrain the tracheal trunk. To test this hypothesis, we first measured the dorsal tracheal trunk position relative to the midline in wild-type larvae (Fig. 5; Fig. S8). The larval length varies from fully elongated at the beginning of a stride cycle to compacted during the somatic peristaltic wave and visceral piston phase. We observed that dorsal tracheal trunks are more curved at the end of each peristaltic wave, with two conspicuous curves located in the thoracic and abdominal regions, respectively (Fig. S8). AMs A2-A5 roughly frame the major, abdominal curvature (Fig. 5D). Upon AM elimination, the double tracheal curvature is still observed. However, the abdominal curve is larger and the dorsal trachea more distant from the midline (Fig. 5B-D; Fig. S8). These results indicate that AMs constrain the tracheal position during larval crawling.

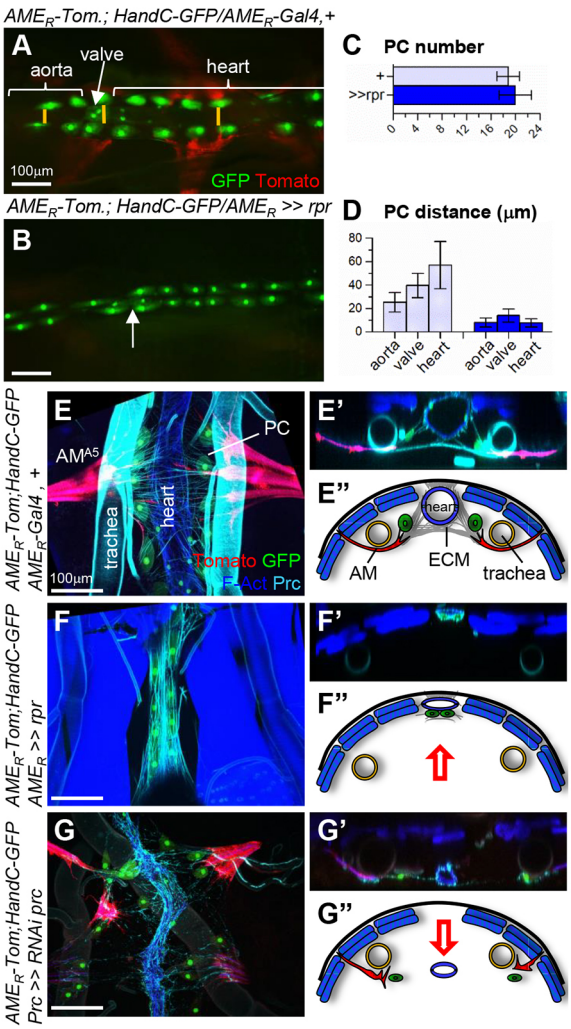

Fig. 4. AMs maintain heart intra-celomic position and lumen opening. (A,B) Dorsal views of the AM$^{A4\text{-}A6}$ region of intact *AME$_R$-cd4-tdTomato; HandC-GFP, AME$_R$-Gal4* (A) and *>>UAS-rpr* (B) larvae. AMs and TARMs are in red and PCs, cardioblasts and valve cells in green. Arrow in A and B indicates the valve position. (C) The number of PCs is unchanged in control and following AM ablation. (D) Distance separating left and right PCs at three positions (yellow bars in A), aorta, valve and heart chamber, in control and following AM ablation. Bar graphs show mean±s.d. (*n*=10 larvae). (E-G″) Semi-intact *AME$_R$-cd4-tdTomato; HandC-GFP, AME$_R$-Gal4* (E), *>>UAS-rpr* (F) and *AME$_R$-cd4-tdTomato; HandC-GFP/prc-Gal4, UAS-RNAi-prc* (G) larvae stained for F-Actin and Prc. PCs and cardioblasts are green, AMs red, somatic muscles and heart blue, the ECM and trachea cyan. E′-G′ show transversal views. (E″-G″) Schematic representations adapted from the images in E′-G′ showing the relative positions of AMs, ECM, heart, PCs and the tracheal trunks. Red arrows indicate the shift in dorsoventral position of the heart. Scale bars: 100 µm.

TARMs are essential for gut and gastric caeca positioning and food transit

A142-GFP expression allows visualisation of the Pv, Gc, anterior loop of the gut and positioning of the visceral mass. Upon removal of either TARMs (*AME$_R$>>Antp*) or TARMs plus AMs (*AME$_R$>>rpr*), there is a posterior shift in the position of the first gut loop and visceral mass (Fig. 6A-C′; Table S2), suggesting that TARM^{T2} connection to the midgut is required for maintaining the proper position of the visceral system in the body cavity. In addition, the dorsal Gcs, which normally extend anterior-wards by attaching to TARM^{T1} (9/10 larvae), now coil around the proventriculus (14/14 larvae) (Fig. 6D-E′). We then tested whether removal of

Development (2020) 147, dev185645. doi:10.1242/dev.185645

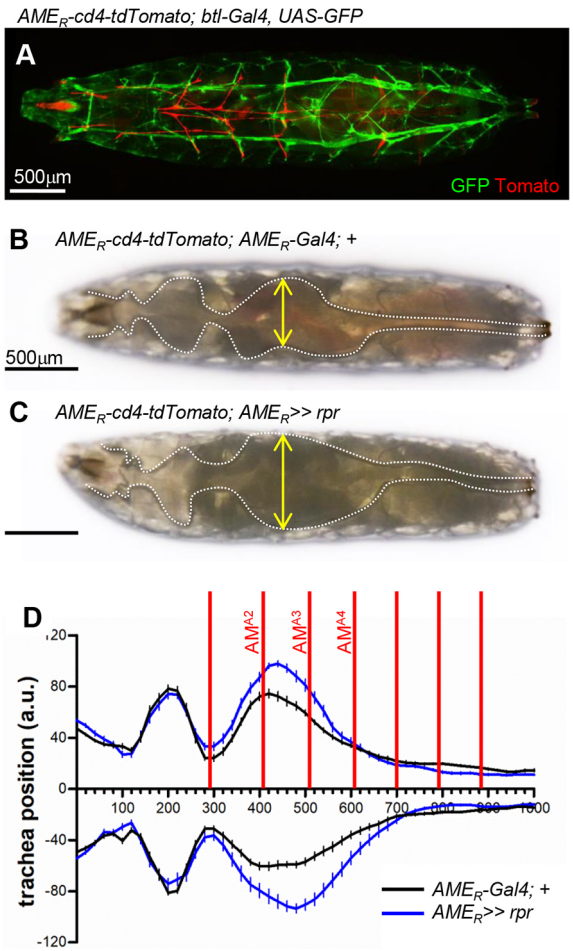

Fig. 5. AMs constrain the tracheal curvature in larvae. (A) Dorsal view of a fully elongated *AME$_R$-cd4-tdTomato; btl-Gal4, UAS-GFP* L3 larva. AMs and TARMs are in red and trachea in green. (B,C) Dorsal views of *AME$_R$-cd4-tdTomato; AME$_R$-Gal4* (B) and *>>rpr* (C) larvae. The tracheal trunk, seen in brightfield, is outlined in white, and spacing indicated by yellow double arrows. (D) Tracheal curvatures in *AME$_R$-Gal4* (black lines) and *>>rpr* (blue lines) L3 larvae at the end of a peristaltic wave. Mean±s.e.m. are given (*n*=15 larvae). AM^{A1} to AM^{A7} positions are indicated by red lines. Scale bars: 500 µm.

AMs had a global impact on food transit through the midgut, using a Bromophenol Blue food ingestion assay. Absence of TARMs significantly reduces the amount of ingested food (Fig. 6F,G). We conclude that TARMs are required for maintaining visceral organ positioning in the larva, insuring efficient food transit inside the gut.

DISCUSSION

Drosophila organogenesis, along with morphogenesis during embryonic development, ends with larval hatching. In most textbooks, development of each larval organ is considered separately, even though interactions between different germ layers, tissues or cell types are referenced. Here, we show that, during larval life, multiple internal organs remain physically connected to the exoskeleton by a web of thin and deformable muscles, the AMs and TARMs (Fig. 7). These atypical, asymmetrically attached muscles are required to maintain proper position of cardiac, visceral and tracheal organs within the coelomic cavity, and heart lumen opening, and, thus, are important physiological regulators.

AM/TARM targeting to different organs: Hox input

Establishment of the muscle pattern, i.e. positions and orientations of each skeletal muscle relative to the other, involves positional values in the epidermis in each body segment. Targeting specific epidermal attachment sites and muscle-muscle matching are intrinsic properties of developing muscle, under the control of iTFs (de Joussineau et al., 2012). We show here that attachment of AMs and TARMs to either the circulatory or the visceral system is under intrinsic Hox control. TARM^{T2} does not express any homeotic gene of the *Antp* or *bithorax* complex, extending to AMs the previous conclusion that the T2 muscle pattern could represent a ground state for the somatic mesoderm (Roy et al., 1997). However, TARM^{T2} specifically connects to the first midgut constriction, where Antp-expressing cells are specified and required for this constriction to form (Reuter and Scott, 1990). In homeotic *Ubx* mutants, AM^{A1} and AM^{A2} are transformed into TARM^{T2}-like muscles, which connect to the same specific gut constriction as normal TARM^{T2}. We thus infer that the background state of AM/TARM attachment is the gut and that targeting information is provided by midgut regionalisation. The guidance cues remain to be identified. MT anchoring of AM^{A3} is also driven by MT tip cell properties rather than homeotic identity of the AM (Weavers and Skaer, 2013). Altogether, these findings show that the unusual morphology and connections of TARMs and AMs both depend upon iTF and Hox intrinsic information, and guidance cues from internal organs.

Specific morphologies and internal organ connections of AMs

Posterior AMs (A5-A7) connected to the heart chamber display a similar fan-like morphology in larvae and adults. Literature on the physiology of the insect adult heart pointed to the absence of a consistent link between AM contraction and heart-beating rates, and severing of AMs could result in a heart chamber collapse (Jones, 1954; Bullock and Horridge, 1965). More recent studies on adult mosquitos suggested that tension exerted by AMs causes an expansion of the heart cross-sectional area (Glenn et al., 2010). Genetic ablations show that AMs are indeed both required for maintaining the heart in the proper haemocelic position and for opening of the heart chamber, but not for heart beating. AMs do not directly bind to cardiomyocytes but to the ECM surrounding PCs, reminiscent of attachment of the diaphragm to the pericardium, a mesothelial monolayer that equalises gravitational, hydrostatic and inertial forces over the surface of the vertebrate heart (Hoit, 2017). During metamorphosis, anterior AMs dedifferentiate into mononucleate myoblasts, which later form ventral longitudinal muscles, a component of the 'dorsal diaphragm' covering the ventral surface of the adult dorsal vessel (Schaub et al., 2015).

Anterior AMs (segments A1-A4) adopt a conspicuous 'T' shape during larval development, with myofibres oriented ventrodorsally from the exoskeleton to the aorta, then laterally along the aorta. The functional role of this 'T'-shape morphology remains unknown. Lateral branches of AM$^{A1\text{-}A3}$ run along LG lobes (Fig. 7A). This geometry and presence in the aorta of vesicles originating from AMs raises the possibility that, in addition to a mechanical support function, AMs could play a signalling role in haematopoiesis.

AMs contact different organs in their trajectory from the exoskeleton to the heart (Fig. 7A). AM^{A3} adhesion to the anterior MT tip cell and positioning of AM^{A4} and AM^{A5} anterior and posterior to the gonad, respectively, are established during embryogenesis. Whereas AM^{A3} is required to anchor the MT (Weavers and Skaer, 2013), the germ cell/niche assembly is independent of AMs (Anllo et al., 2019). Several AMs send projections to fat body, including AM^{A4} and AM^{A5}, which project

Development (2020) 147, dev185645. doi:10.1242/dev.185645

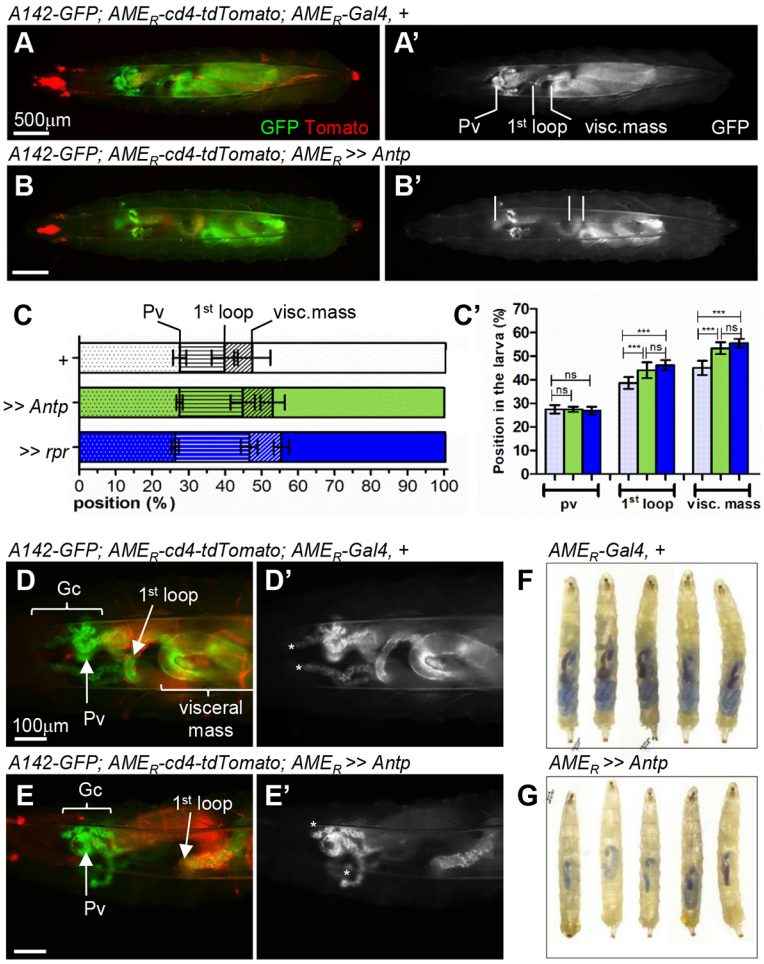

Fig. 6. TARMs are required for proper topology of visceral organs and food transit. (A-B′) Dorsal views of intact *A142-GFP; AME$_R$-cd4-tdTomato; AME$_R$-Gal4* (A) and *>>UAS-Antp* (B) larvae. AMs and TARMs are red, visceral organs green. A′ and B′ show only the visceral system. (C,C′) Relative positions (percentage of larva length) of the Pv, first midgut loop and visceral mass in controls and following TARM ablation. Bar graphs show mean±s.d. (n=10 larvae). (D-E′) Magnified views of the anterior region of *A142-GFP; AME$_R$-cd4-tdTomato; AME$_R$-Gal4* (D) and *>>Antp* (E) larvae. D′ and E′ show the GFP channel only. (D,D′) TARM^{T1} maintains Gc extension (asterisk; $n\geq10$); TARM^{T2} connects to the first loop of the gut. Upon TARM ablation (E,E′), Gcs coil around the Pv, and the first midgut loop is shifted posteriorly. (F,G) Ventral views of *AME$_R$-cd4-tdTomato; AME$_R$-Gal4* (F) and *>>Antp* (G) larvae fed 45 min with blue yeast. Anterior at the top (n>25). Scale bars: 500 µm in A,B; 100 µm in D,E.

to the fat body surrounding the male gonad. Whether AM segment-specific projections play architectural and/or signalling roles via the release of diffusible signals similar to myokines in vertebrates (Das et al., 2019) remains to be fully assessed. The multiple shapes adopted by AMs suggest that they could be passively deformed by the steric volume of internal organs during larval crawling. Conversely, lateral 'floating' of the dorsal tracheal branches and dorsal shifting of the heart in the absence of AMs shows that the internal architecture of the larva is constrained by AMs.

TARM-midgut connections are required for efficient visceral system activity

TARMs (Fig. 7) were only recently discovered in the *Drosophila* embryo and both their phylogenic spread and fate in adults remain to be explored. Ablation of TARMs prevents unfolding of the dorsal Gc and provokes a posterior shift of the midgut position. Little is known about the precise role of the Gc, which could act as an exocrine organ in synthesising and secreting digestive enzymes in *Drosophila* (Matsumoto et al., 1995; Grönke et al., 2005) and osmoregulation in *Aedes* and *Anopheles* larvae (Volkmann and Peters, 1989; D'Silva and O'Donnell, 2018). TARM^{T1} attachment raises further questions, of whether dorsal caeca play specific roles, and which roles require extended shape and/or TARM^{T1} connection. TARM^{T2} attaches to the midgut where DH31-expressing enteroendocrine cells are located. DH31 cells are required for peristalsis of the anterior midgut (LaJeunesse et al., 2010). The finding that TARM ablation reduces the transit of food through the midgut suggests two, not mutually exclusive, interpretations: the loss of the first midgut loop impairs peristalsis and/or loss of the TARM^{T2} connection to DH31-expressing cells leads to dysregulation of enteroendocrine functions.

Neither cardiac, nor visceral or skeletal: a novel type of Tbx1/Islet1-expressing muscles

The recent discovery of TARMs was an unanticipated outcome of the characterisation of Org-1 and Islet1 transcription enhancers (Schaub et al., 2012; Boukhatmi et al., 2012, 2014), that allowed live imaging of AMs and TARMs in larvae. Being multinucleated and striated, *Drosophila* AMs and TARMs resemble skeletal muscles, correlating with a related mode of embryonic development (Boukhatmi et al., 2014). However, they exhibit features that distinguish them from body wall muscles. One is their morphology and deformation properties. It will be interesting to determine whether specific MHC isoforms (George et al., 1989) and/or proteins of Z-discs, the sarcomere anchors in striated muscles (Luther, 2009; Steinmetz et al., 2012), are expressed in either TARMs or AMs.

Another AM/TARM-specific feature is their asymmetric attachment, to the exoskeleton and soft tissues at the other. In primates, asymmetric attachment has been observed for facial subcutaneous muscles, which insert into the skin on one side and to facial bones or other muscles on the other (Ziermann et al., 2018). Facial muscles derive in part from cardiopharyngeal mesoderm, also at the origin of the oesophagus striated muscle (ESM) (Gopalakrishnan et al., 2015; Heude et al., 2018). ESM development is regulated by *Tbx1* and *Islet1*, *Tbx1* acting genetically upstream of *Isl1* in ESM

Development (2020) 147, dev185645. doi:10.1242/dev.185645

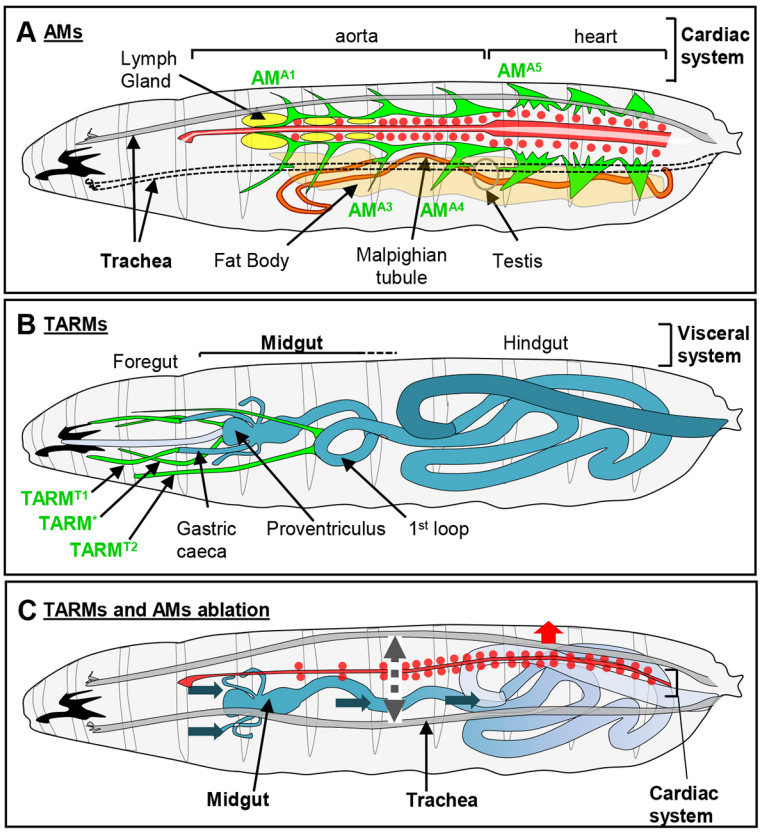

Fig. 7. TARMs and AMs maintain the positions of internal organs in larva. (A-C) Schematics of a fully extended L3 larva (adapted from Hartenstein, 1993). (A) AM connections to the cardiac system (red), LG (yellow), anterior MTs (orange) and fat body (beige), and surrounding of trachea (grey). (B) TARM connections to specific midgut regions (blue). (C) Mis-positioning of multiple internal organs following TARM/AM elimination, as indicated by arrows: Gc and visceral mass (blue arrows), heart (red arrow) and dorsal trachea (dashed grey arrow). The heart lumen is collapsed.

progenitors (Gopalakrishnan et al., 2015; Comai et al., 2019). The Tbx1/Islet genetic hierarchy controls *Drosophila* AM/TARM development (Boukhatmi et al., 2014) and is redeployed during metamorphosis to initiate transdifferentiation of some AMs into the ventral longitudinal muscles of the adult heart (Schaub et al., 2015). Whether this genetic cascade has been independently recruited in mammals and insects for diversification and specific adaptations of striated muscles is an open question.

The diaphragm, which separates lung and heart from visceral organs in mammals, is also an asymmetric muscle. Its C-shape results from insertion of muscular fibres to, on one side, a sheet of fibrous tissue, the central tendon, which surrounds the oesophageal hiatus, and, on the other, tendinous tissue surrounding ribs and vertebrae (Merrell and Kardon, 2013). Although highly speculative, whether the mammalian diaphragm and the insect AMs/TARMs could represent two specific adaptations of an ancestral demarcation between circulatory, respiratory and visceral organs, is a possibility.

Conclusions and perspectives

To the best of our knowledge, TARMs and AMs are the first example of multinucleate striated muscles connecting the (exo)skeleton to internal organs in bilaterians. Characterisation of a new type of striated muscles raises novel anatomical, physiological and evolutionary questions. Innervation of the heart and AMs in adult arthropods remains controversial (Dulcis and Levine, 2003). Extant reports of embryonic and larval AM innervation concluded that AMs are innervated by a peripheral neuron, the lateral-bidendritic neuron or a motoneuron, or both (Gorczyca et al., 1994; Landgraf and Thor, 2006). Innervation by sensory neurons would raise the exciting possibility that AMs/TARMs are part of internal proprioceptive circuits. Integrating neuromuscular connectivity into physiological roles of TARMs and AMs is the next challenge.

MATERIALS AND METHODS

Drosophila strains

All *Drosophila melanogaster* stocks and crosses were grown on standard medium at 25°C. Strains used were: *AME-moeGFP* (Boukhatmi et al., 2012), *A142-GFP* (Buchon et al., 2013), *HandC-GFP* (Sellin et al., 2006), *UAS-H2bRFP* (Zobeck et al., 2010), *fTRG500-MHC-GFP, fTRG569-Kettin/sls-GFP, fTRG1046-Unc-89-GFP* (Sarov et al., 2016), *Prc-Gal4* (Chartier et al., 2002), *UAS-Ubx* (Michelson, 1994), *org-1-LacZ* (Schaub et al., 2012), *Pcol85-Gal4* (Krzemień et al., 2007), *domeMESO-GFP* (Oyallon et al., 2016), *FB-Gal4* (gift from M. Meister, Institut de Biologie Moléculaire et Cellulaire, UPR 9022 CNRS, Strasbourg, France; Grönke et al., 2003), *btl-Gal4* (gift from J. Casanova, Institute for Research in Biomedicine, IBMB-CSIC, Barcelona, Spain) and *sr-Gal4* (obtained from T. Volk, Weizmann Institute of Science, Rehovot, Israel). The following strains were obtained from the Bloomington *Drosophila* Stock Center: *UAS-cd4-tdTomato* (BDSC:35841), *UAS-cd4-tdGFP* (BDSC:35836), *UAS-mcd8GFP* (BDSC:5137), *UAS-mIFP* (BDSC:64183), *20xUAS-GCaMP3* (BDSC:32235), *Cha-Gal4* (BDSC:6793), *Ilk-GFP^{ZCL3111}* (BDSC:6831), *how^{24B}-Gal4* (BDSC:1767), *UAS-Antp* (BDSC:7301), *Ubx$^{9.22}$* (BDSC:3474), *UAS-rpr* (BDSC:5824) and *UAS-RNAi-prc* (BDSC:65898). *Zasp66^{ZCL0663}* was obtained from the Kyoto Stock Center.

Lethal stocks were balanced using *CyO*,{*dfd-YFP*}, *TM6*,{*dfd-YFP*} or *TM3*, *Ser*,{*twi-lacZ*} and mutant embryos or larvae identified by absence of *lacZ* or YFP expression, respectively.

Constructions of transgenic reporter lines

For constructing AM/TARM-specific reporter and Gal4 lines, we shortened the *tup-AME* enhancer (Boukhatmi et al., 2014), based on the position of Org-1 binding sites and conserved sequence blocks. *tup-AME$_R$* DNA, corresponding to the *tup* upstream region, chr2L positions: 18900307..18899855 (FlyBase; release R6.32), was amplified from *yw* genomic DNA using the primers 5′-ATCCGCTGCTGCTGCATC-3′ and 5′-GCCGAGCAAGTACTAAGTACC-3′. The amplified 452 bp fragment was cloned into pENTR4 (Gateway cloning system; Invitrogen) to give the donor plasmid pDONR-AME$_R$, which was recombined, using

Development (2020) 147, dev185645. doi:10.1242/dev.185645

LR recombinase (Invitrogen), with pDEST-Gal4, pDEST-HemmarG (Addgene-plasmid #31221) and pDEST-HemmarR (Addgene-plasmid #31222), to give pEXP-AME$_R$-Gal4, pEXP-AME$_R$-tdGFP and pEXP-AME$_R$-cd4-tdTomato. Transgenes were inserted at position 25C6 on the second chromosome (AME$_R$-cd4-tdTomato), or 99F8 (AME$_R$-cd4-tdTomato and GFP) or 68A4 (AME$_R$-Gal4) on the third chromosome, by injection into attP embryos (BDSC: 25709, BDSC: 24867, nos-phiC31-NLS; attP2, respectively) (Bischof et al., 2007; Markstein et al., 2008).

Immunohistochemistry of whole-mount embryos and semi-intact L3 preparation

Immunostainings of whole-mount embryos were performed using standard techniques, as described previously (Dubois et al., 2016); third instar larvae dissection and staining were as described (Drechsler et al., 2013).

The following primary antibodies were used: chicken anti-GFP (1:500; Abcam, ab13970) and anti-β-galactosidase (1:2000; Abcam, 9361); rabbit anti-Scr (1:400; courtesy of David Cribbs, Centre de Biologie Intégrative, Toulouse, France), anti-cleaved Dcp1 (1:200; Cell Signaling Technologies, #9578), anti-β3-Tub (1:5000; Renate Renkawitz-Pohl, Philipps-Universität Marburg, Fachbereich Biologie, Entwicklungsbiologie, Marburg, Germany), anti-Mesh (1:1000) (Izumi et al., 2012); mouse anti-Antp [1:100; Developmental Studies Hybridoma Bank (DSHB), 8C11], anti-Ubx (1:50; DSHB, FP3.38), anti-AbdB (1:50; DSHB, 1A2E9), anti-FasIII (1:20; DSHB, 7G10); anti-GFP (1:100; Roche, 11 814 460 001), anti-Prc (1:200; DSHB, EC11); and rat anti-TM (1:500; Abcam, ab50567). Phalloidin-647 (1/200) and Texas RedX (1/500) were obtained from Thermo Fisher Scientific (A22287 and T7471, respectively). Secondary antibodies were Alexa Fluor 405-, 488-, 647-, 555-conjugated antibodies (1:300; Thermo Fisher Scientific, A-31553, A-11001, A-11034, A-11039, A-21434, A-21437, A-21235 and A-21244).

Optimised confocal sections were acquired using Zeiss710 or Leica SPE microscopes. Projections and 3D reconstructions were created using ImageJ, Fiji and Imaris software.

Imaging of entire immobilised larva

To image fully extended, translucent, immobilised larvae, larvae were drowned in water for 1 h. Larvae placed between the slide and coverslip were imaged using a Leica SPE microscope, a Nikon AZ100 466 Macroscope at 2× or 5× objective plus optical zoom, or a Nikon SMZ18 Macroscope for brightfield colour images. Mosaic acquisitions and image reconstructions of some entire larvae were performed to improve focus and resolution.

Time-lapse imaging of larva

For time-lapse imaging, late L2 or early L3 GFP larva were mounted between the slide and coverslip with a small drop of water. Image series were acquired using a Nikon AZ100 466 Macroscope, with the following settings: objective ×5, zoom ×1.25, time exposure: 30 ms, 30 fps (Movie 1) or 150 ms, 5 fps (Movie 3); objective ×2, zoom ×1.25; time exposure: 100 ms, 10 fps (Movie 2). Ca^{2+} waves in AMs (Fig. 3F-G′, Movie 3) were imaged in *AME$_R$-cd4-tdTomato; AME$_R$-Gal4; 20xUAS-GCaMP3* early L3 larvae immobilised by pressure to prevent crawling. The filters were manually changed during the mono-colour acquisition to successively visualise the muscle shape with Tomato and intracellular calcium rise with GCaMP-GFP. Movies were processed using HCImage Live and Fiji software.

Feeding assay

Feeding L3 larvae were collected and transferred to a 1% agarose plate covered with a thin layer of blue yeast paste (0.5 g/ml baker's yeast, 0.005 g/ml Bromophenol Blue in water) for 45 min at a density of 20 larvae/plate. Larvae were then washed and fixed by heat (5 s at 65°C) and imaged from the ventral side using a Nikon SMZ18 Macroscope.

Quantification of embryonic, larval and pupal viability

The numbers of embryos laid for 8 h on an agar plate, and unhatched embryos 36 h later, were counted to determine embryonic viability (two independent counts for each genotype; n_{min}=509, n_{max}=725 embryos). For larval viability, L1 larvae collected 24 h after egg deposition (8 h egg collections) were gently transferred into fly food tubes (30 L1/tube; n_{min}=240, n_{max}=510 L1) and the number of resulting pupae was counted. Pupal viability corresponds to the percentage of pupae developing to adults (n_{min}=37; n_{max}=347 pupa).

Quantification of PC number and distance between PCs

Entire immobilised *HandC-GFP* larvae were imaged using a Nikon AZ100 466 Macroscope. The number of PCs per hemi-larva, visualised with GFP, were manually counted (n_{min}=20 hemi-larvae). For each genetic condition, the mean number of PCs±s.d. is given. The distance between left and right PCs was measured at three distinct positions – aorta, valve and heart – using Fiji software. For each genetic condition, the mean distance between PCs ±s.d. is given (n_{min}=10 larva).

Quantification of heart beating in white pupa

PCs were visualised in *HandC-GFP* white pupae. A Nikon AZ100 466 Macroscope was used to record heart beating (objective ×5, zoom ×1.25; time exposure: 100 ms, 10 fps, 20 s, two repetitions for each pupa). Heart pulses were then manually counted (n=12 pupa for each genotype).

Quantification of trachea position in entire larva

L3 feeding larvae were collected and transferred onto 1% agarose plates. Larva were filmed using a Nikon SMZ18 Macroscope (brightfield; zoom ×0.75; 10 fps) and for each larva, the image corresponding to the tracheal distortion step was extracted using Fiji. The left and right dorsal trunk paths from anterior to posterior spiracles and the midline were manually drawn. To standardise the data, the three lines were normalised to a fixed value of 1000 from anterior to posterior spiracles. A homemade C program (available on request) using MagickWand API (ImageMagick) allowed us to extract *xy* coordinates. Relative *y* positions of left and right trachea, for *y* midline position=0, were calculated. Excel was used to calculate the mean tracheal position and the s.d. (n=15 larva for each genotype).

Quantification of visceral system position in entire larva

The visceral system was visualised using *A142-GFP* on entire immobilised larvae. The larvae size and positions of the proventriculus (Pv), first loop of the gut and visceral mass, respectively, were measured using Fiji software. The relative positions of Pv, first loop and visceral mass, were calculated (%) relative to the larva size normalised to 100%. For each genetic condition, the mean larva size and the mean relative positions±s.d. are given (n=10 larva).

Statistical analysis

For all experiments, data plots and statistical analyses were performed with Prism 5.0. Mean values are shown, error bars represent s.d. or s.e.m. as indicated in figure legends. For statistical comparisons, unpaired *t*-test or one-way analysis of variance and Tukey post-tests were used, where appropriate. Asterisks show the significance of variation (ns, not significant; ***P<0.001).

Acknowledgements

We thank the Bloomington and Kyoto Stock Centers and colleagues for *Drosophila* strains and antibodies. We thank Michèle Crozatier, Alice Davy and Cédric Polesello for helpful discussion and critical reading of the manuscript. We acknowledge the help from the Toulouse RIO Imaging platform, Marine Mercier, Ismael Morin-Poulard and Julien Favier for fly stocks and Benoît Condoumy for computer image analysis.

Competing interests

The authors declare no competing or financial interests.

Author contributions

Conceptualization: L.B., A.V.; Methodology: L.B., A.V.; Validation: L.B., A.V.; Formal analysis: L.B.; Investigation: L.B., N.C., A. Pelletier, J.-L.F., A.V.; Resources: A. Paululat, G.L., Y.C., J.-L.F.; Writing - original draft: L.B., A.V.; Writing - review & editing: L.B., A.V.; Visualization: L.B., A.V.; Project administration: L.B., A.V.; Funding acquisition: L.B., A. Paululat, A.V.

Funding

This work was supported by the Centre National de la Recherche Scientifique, the Institut National de la Santé et de la Recherche Médicale, the Ministère de l'Enseignement supérieur, de la Recherche et de l'Innovation, the Association

Française contre les Myopathies (AFM) (21887), the Agence Nationale de la Recherche (13-BSVE2-0010-0 to A.V.), Campus France (PHC PROCOPE 2017 to L.B. and A. Paululat), and the Deutsche Forschungsgemeinschaft (SFB944, PA 14-1 to A. Paululat).

Supplementary information

Supplementary information available online at
http://dev.biologists.org/lookup/doi/10.1242/dev.185645.supplemental

References

Anllo, L., Plasschaert, L. W., Sui, J. and DiNardo, S. (2019). Live imaging reveals hub cell assembly and compaction dynamics during morphogenesis of the *Drosophila* testis niche. *Dev. Biol.* **446**, 102-118. doi:10.1016/j.ydbio.2018.12.014

Armand, P., Knapp, A. C., Hirsch, A. J., Wieschaus, E. F. and Cole, M. D. (1994). A novel basic helix-loop-helix protein is expressed in muscle attachment sites of the *Drosophila* epidermis. *Mol. Cell. Biol.* **14**, 4145-4154. doi:10.1128/MCB.14.6.4145

Bataillé, L., Frendo, J.-L. and Vincent, A. (2015). Hox control of *Drosophila* larval anatomy; the alary and thoracic alary-related muscles. *Mech. Dev.* **138**, 170-176. doi:10.1016/j.mod.2015.07.005

Bate, M. and Rushton, E. (1993). Myogenesis and muscle patterning in *Drosophila*. *C. R. Acad. Sci. III* **316**, 1047-1061.

Bischof, J., Maeda, R. K., Hediger, M., Karch, F. and Basler, K. (2007). An optimized transgenesis system for *Drosophila* using germ-line-specific phiC31 integrases. *Proc. Natl. Acad. Sci. USA* **104**, 3312-3317. doi:10.1073/pnas.0611511104

Boukhatmi, H., Frendo, J. L., Enriquez, J., Crozatier, M., Dubois, L. and Vincent, A. (2012). Tup/Islet1 integrates time and position to specify muscle identity in Drosophila. *Development* **139**, 3572-3582. doi:10.1242/dev.083410

Boukhatmi, H., Schaub, C., Bataillé, L., Reim, I., Frendo, J.-L., Frasch, M. and Vincent, A. (2014). An Org-1-Tup transcriptional cascade reveals different types of alary muscles connecting internal organs in Drosophila. *Development* **141**, 3761-3771. doi:10.1242/dev.111005

Buchon, N., Osman, D., David, F. P. A., Fang, H. Y., Boquete, J.-P., Deplancke, B. and Lemaitre, B. (2013). Morphological and molecular characterization of adult midgut compartmentalization in Drosophila. *Cell Rep.* **3**, 1725-1738. doi:10.1016/j.celrep.2013.04.001

Buckingham, M. (2017). Gene regulatory networks and cell lineages that underlie the formation of skeletal muscle. *Proc. Natl. Acad. Sci. USA* **114**, 5830-5837. doi:10.1073/pnas.1610605114

Buechling, T., Akasaka, T., Vogler, G., Ruiz-Lozano, P., Ocorr, K. and Bodmer, R. (2009). Non-autonomous modulation of heart rhythm, contractility and morphology in adult fruit flies. *Dev. Biol.* **328**, 483-492. doi:10.1016/j.ydbio.2009.02.013

Bullock, T. H. and Horridge, G. A. (1965). *Structure and Function in the Nervous Systems of Invertebrates*. San Francisco: W.H. Freeman.

Chartier, A., Zaffran, S., Astier, M., Sémériva, M. and Gratecos, D. (2002). Pericardin, a Drosophila type IV collagen-like protein is involved in the morphogenesis and maintenance of the heart epithelium during dorsal ectoderm closure. *Development* **129**, 3241-3253.

Choma, M. A., Suter, M. J., Vakoc, B. J., Bouma, B. E. and Tearney, G. J. (2011). Physiological homology between Drosophila melanogaster and vertebrate cardiovascular systems. *Dis. Model. Mech.* **4**, 411-420. doi:10.1242/dmm.005231

Comai, G., Heude, E., Mella, S., Paisant, S., Pala, F., Gallardo, M., Langa, F., Kardon, G., Gopalakrishnan, S. and Tajbakhsh, S. (2019). A distinct cardiopharyngeal mesoderm genetic hierarchy establishes antero-posterior patterning of esophagus striated muscle. *eLife* **8**, e47460. doi:10.7554/eLife.47460

Curtis, N. J., Ringo, J. M. and Dowse, H. B. (1999). Morphology of the pupal heart, adult heart, and associated tissues in the fruit fly, Drosophila melanogaster. *J. Morphol.* **240**, 225-235. doi:10.1002/(SICI)1097-4687(199906)240:3<225::AID-JMOR2>3.0.CO;2-V

Das, D. K., Graham, Z. A. and Cardozo, C. P. (2019). Myokines in skeletal muscle physiology and metabolism: recent advances and future perspectives. *Acta Physiol. (Oxf.)* **228**, e13367. doi:10.1111/apha.13367

de Joussineau, C., Bataillé, L., Jagla, T. and Jagla, K. (2012). Diversification of muscle types in Drosophila: upstream and downstream of identity genes. *Curr. Top. Dev. Biol.* **98**, 277-301. doi:10.1016/B978-0-12-386499-4.00011-2

Drechsler, M., Schmidt, A. C., Meyer, H. and Paululat, A. (2013). The conserved ADAMTS-like protein lonely heart mediates matrix formation and cardiac tissue integrity. *PLoS Genet.* **9**, e1003616. doi:10.1371/journal.pgen.1003616

D'Silva, N. M. and O'Donnell, M. J. (2018). The gastric caecum of larval. *J. Exp. Biol.* **221**, jeb172866. doi:10.1242/jeb.172866

Dubois, L., Frendo, J.-L., Chanut-Delalande, H., Crozatier, M. and Vincent, A. (2016). Genetic dissection of the Transcription Factor code controlling serial specification of muscle identities in Drosophila. *eLife* **5**, e14979. doi:10.7554/eLife.14979

Dulcis, D. and Levine, R. B. (2003). Innervation of the heart of the adult fruit fly, Drosophila melanogaster. *J. Comp. Neurol.* **465**, 560-578. doi:10.1002/cne.10869

Ejaz, A. and Lange, A. B. (2008). Peptidergic control of the heart of the stick insect, Baculum extradentatum. *Peptides* **29**, 214-225. doi:10.1016/j.peptides.2007.07.036

George, E. L., Ober, M. B. and Emerson, C. P. (1989). Functional domains of the Drosophila melanogaster muscle myosin heavy-chain gene are encoded by alternatively spliced exons. *Mol. Cell. Biol.* **9**, 2957-2974. doi:10.1128/MCB.9.7.2957

Glenn, J. D., King, J. G. and Hillyer, J. F. (2010). Structural mechanics of the mosquito heart and its function in bidirectional hemolymph transport. *J. Exp. Biol.* **213**, 541-550. doi:10.1242/jeb.035014

Gopalakrishnan, S., Comai, G., Sambasivan, R., Francou, A., Kelly, R. G. and Tajbakhsh, S. (2015). A cranial mesoderm origin for esophagus striated muscles. *Dev. Cell* **34**, 694-704. doi:10.1016/j.devcel.2015.07.003

Gorczyca, M. G., Phillis, R. W. and Budnik, V. (1994). The role of tinman, a mesodermal cell fate gene, in axon pathfinding during the development of the transverse nerve in Drosophila. *Development* **120**, 2143-2152.

Grönke, S., Beller, M., Fellert, S., Ramakrishnan, H., Jäckle, H. and Kühnlein, R. P. (2003). Control of fat storage by a Drosophila PAT domain protein. *Curr. Biol.* **13**, 603-606. doi:10.1016/S0960-9822(03)00175-1

Grönke, S., Mildner, A., Fellert, S., Tennagels, N., Petry, S., Müller, G., Jäckle, H. and Kühnlein, R. P. (2005). Brummer lipase is an evolutionary conserved fat storage regulator in Drosophila. *Cell Metab.* **1**, 323-330. doi:10.1016/j.cmet.2005.04.003

Hartenstein V. (1993). Atlas of Drosophila Development, in *The Development of* Drosophila melanogaster, (ed. M. Bate and A. Martinez-Arias). Cold Spring Harbor, NY: Cold Spring Harbor Laboratory Press.

Heckscher, E. S., Lockery, S. R. and Doe, C. Q. (2012). Characterization of Drosophila larval crawling at the level of organism, segment, and somatic body wall musculature. *J. Neurosci.* **32**, 12460-12471. doi:10.1523/JNEUROSCI.0222-12.2012

Heude, E., Tesarova, M., Sefton, E. M., Jullian, E., Adachi, N., Grimaldi, A., Zikmund, T., Kaiser, J., Kardon, G., Kelly, R. G. et al. (2018). Unique morphogenetic signatures define mammalian neck muscles and associated connective tissues. *eLife* **7**, e40179. doi:10.7554/eLife.40179

Hoit, B. D. (2017). Anatomy and Physiology of the Pericardium. *Cardiol. Clin.* **35**, 481-490. doi:10.1016/j.ccl.2017.07.002

Hudson, A. M., Petrella, L. N., Tanaka, A. J. and Cooley, L. (2008). Mononuclear muscle cells in Drosophila ovaries revealed by GFP protein traps. *Dev. Biol.* **314**, 329-340. doi:10.1016/j.ydbio.2007.11.029

Hwang, R. Y., Zhong, L., Xu, Y., Johnson, T., Zhang, F., Deisseroth, K. and Tracey, W. D. (2007). Nociceptive neurons protect Drosophila larvae from parasitoid wasps. *Curr. Biol.* **17**, 2105-2116. doi:10.1016/j.cub.2007.11.029

Izumi, Y., Yanagihashi, Y. and Furuse, M. (2012). A novel protein complex, Mesh-Ssk, is required for septate junction formation in the Drosophila midgut. *J. Cell Sci.* **125**, 4923-4933. doi:10.1242/jcs.112243

Jones, J. C. (1954). The heart and associated tissues of *Anopheles quadrimaculatus* Say (Diptera: Culicidae). *J. Morphol.* **94**, 71-123. doi:10.1002/jmor.1050940104

Krzemień, J., Dubois, L., Makki, R., Meister, M., Vincent, A. and Crozatier, M. (2007). Control of blood cell homeostasis in Drosophila larvae by the posterior signalling centre. *Nature* **446**, 325-328. doi:10.1038/nature05650

LaBeau, E. M., Trujillo, D. L. and Cripps, R. M. (2009). Bithorax complex genes control alary muscle patterning along the cardiac tube of Drosophila. *Mech. Dev.* **126**, 478-486. doi:10.1016/j.mod.2009.01.001

LaJeunesse, D. R., Johnson, B., Presnell, J. S., Catignas, K. K. and Zapotoczny, G. (2010). Peristalsis in the junction region of the Drosophila larval midgut is modulated by DH31 expressing enteroendocrine cells. *BMC Physiol.* **10**, 14. doi:10.1186/1472-6793-10-14

Landgraf, M. and Thor, S. (2006). Development of Drosophila motoneurons: specification and morphology. *Semin. Cell Dev. Biol.* **17**, 3-11. doi:10.1016/j.semcdb.2005.11.007

League, G. P., Onuh, O. C. and Hillyer, J. F. (2015). Comparative structural and functional analysis of the larval and adult dorsal vessel and its role in hemolymph circulation in the mosquito Anopheles gambiae. *J. Exp. Biol.* **218**, 370-380. doi:10.1242/jeb.114942

Lehmacher, C., Abeln, B. and Paululat, A. (2012). The ultrastructure of Drosophila heart cells. *Arthropod. Struct. Dev.* **41**, 459-474. doi:10.1016/j.asd.2012.02.002

Luther, P. K. (2009). The vertebrate muscle Z-disc: sarcomere anchor for structure and signalling. *J. Muscle Res. Cell Motil.* **30**, 171-185. doi:10.1007/s10974-009-9189-6

Markstein, M., Pitsouli, C., Villalta, C., Celniker, S. E. and Perrimon, N. (2008). Exploiting position effects and the gypsy retrovirus insulator to engineer precisely expressed transgenes. *Nat. Genet.* **40**, 476-483. doi:10.1038/ng.101

Matsumoto, I., Watanabe, H., Abe, K., Arai, S. and Emori, Y. (1995). A putative digestive cysteine proteinase from Drosophila melanogaster is predominantly expressed in the embryonic and larval midgut. *Eur. J. Biochem.* **227**, 582-587. doi:10.1111/j.1432-1033.1995.tb20428.x

Merrell, A. J. and Kardon, G. (2013). Development of the diaphragm – a skeletal muscle essential for mammalian respiration. *FEBS J.* **280**, 4026-4035. doi:10.1111/febs.12274

Michelson, A. M. (1994). Muscle pattern diversification in Drosophila is determined by the autonomous function of homeotic genes in the embryonic mesoderm. *Development* **120**, 755-768.

Noden, D. M. and Francis-West, P. (2006). The differentiation and morphogenesis of craniofacial muscles. *Dev. Dyn.* **235**, 1194-1218. doi:10.1002/dvdy.20697

Oyallon, J., Vanzo, N., Krzemień, J., Morin-Poulard, I., Vincent, A. and Crozatier, M. (2016). Two independent functions of collier/early B cell factor in the control of Drosophila blood cell homeostasis. *PLoS ONE* **11**, e0148978. doi:10.1371/journal.pone.0148978

Pélissier, P., Pistre, V., Bustamante, K., Martin, D. and Baudet, J. (2000). [The modiolus. Comparative anatomy, embryological and physiological review, surgical importance]. *Ann. Chir. Plast. Esthet.* **45**, 41-47.

Reuter, R. and Scott, M. P. (1990). Expression and function of the homoeotic genes Antennapedia and Sex combs reduced in the embryonic midgut of Drosophila. *Development* **109**, 289-303.

Rizki, T. M. (1978). *The Circulatory System and Associated Cells and Tissues*. New York: Academic Press.

Roy, S., Shashidhara, L. S. and VijayRaghavan, K. (1997). Muscles in the Drosophila second thoracic segment are patterned independently of autonomous homeotic gene function. *Curr. Biol.* **7**, 222-227. doi:10.1016/S0960-9822(06)00117-5

Sarov, M., Barz, C., Jambor, H., Hein, M. Y., Schmied, C., Suchold, D., Stender, B., Janosch, S., KJ, V. V., Krishnan, R. T. et al. (2016). A genome-wide resource for the analysis of protein localisation in Drosophila. *eLife* **5**, e12068. doi:10.7554/eLife.12068

Schaub, C., Nagaso, H., Jin, H. and Frasch, M. (2012). Org-1, the Drosophila ortholog of Tbx1, is a direct activator of known identity genes during muscle specification. *Development* **139**, 1001-1012. doi:10.1242/dev.073890

Schaub, C., März, J., Reim, I. and Frasch, M. (2015). Org-1-dependent lineage reprogramming generates the ventral longitudinal musculature of the Drosophila heart. *Curr. Biol.* **25**, 488-494. doi:10.1016/j.cub.2014.12.029

Sellin, J., Albrecht, S., Kölsch, V. and Paululat, A. (2006). Dynamics of heart differentiation, visualized utilizing heart enhancer elements of the Drosophila melanogaster bHLH transcription factor Hand. *Gene Expr. Patterns* **6**, 360-375. doi:10.1016/j.modgep.2005.09.012

Steinmetz, P. R. H., Kraus, J. E. M., Larroux, C., Hammel, J. U., Amon-Hassenzahl, A., Houliston, E., Wörheide, G., Nickel, M., Degnan, B. M. and Technau, U. (2012). Independent evolution of striated muscles in cnidarians and bilaterians. *Nature* **487**, 231-234. doi:10.1038/nature11180

Tao, Y., Wang, J., Tokusumi, T., Gajewski, K. and Schulz, R. A. (2007). Requirement of the LIM homeodomain transcription factor tailup for normal heart and hematopoietic organ formation in Drosophila melanogaster. *Mol. Cell. Biol.* **27**, 3962-3969. doi:10.1128/MCB.00093-07

Tian, L., Hires, S. A., Mao, T., Huber, D., Chiappe, M. E., Chalasani, S. H., Petreanu, L., Akerboom, J., McKinney, S. A., Schreiter, E. R. et al. (2009). Imaging neural activity in worms, flies and mice with improved GCaMP calcium indicators. *Nat. Methods* **6**, 875-881. doi:10.1038/nmeth.1398

Volk, T. (2013). Positioning nuclei within the cytoplasm of striated muscle fiber: cooperation between microtubules and KASH proteins. *Nucleus* **4**, 18-22. doi:10.4161/nucl.23086

Volkmann, A. and Peters, W. (1989). Investigations on the midgut caeca of mosquito larvae-II. Functional aspects. *Tissue Cell* **21**, 253-261. doi:10.1016/0040-8166(89)90070-0

Weavers, H. and Skaer, H. (2013). Tip cells act as dynamic cellular anchors in the morphogenesis of looped renal tubules in Drosophila. *Dev. Cell* **27**, 331-344. doi:10.1016/j.devcel.2013.09.020

Ziermann, J. M., Diogo, R. and Noden, D. M. (2018). Neural crest and the patterning of vertebrate craniofacial muscles. *Genesis* **56**, e23097. doi:10.1002/dvg.23097

Zobeck, K. L., Buckley, M. S., Zipfel, W. R. and Lis, J. T. (2010). Recruitment timing and dynamics of transcription factors at the Hsp70 loci in living cells. *Mol. Cell* **40**, 965-975. doi:10.1016/j.molcel.2010.11.022